PAPER • OPEN ACCESS

# Nonlinear mode coupling and internal resonance observed in a dusty plasma

New Journal of Physics
The open access journal at the forefront of physics

Deutsche Physikalische Gesellschaft DPG
IOP Institute of Physics

Published in partnership with: Deutsche Physikalische Gesellschaft and the Institute of Physics

OPEN ACCESS

RECEIVED
16 August 2019

REVISED
24 September 2019

ACCEPTED FOR PUBLICATION
14 October 2019

PUBLISHED
29 October 2019



PAPER

# Nonlinear mode coupling and internal resonance observed in a dusty plasma

**Zhiyue Ding**[1,2], **Ke Qiao**[2], **Nicholas Ernst**[2], **Jie Kong**[2], **Mudi Chen**[2], **Lorin S Matthews**[1,2] **and Truell W Hyde**[1,2]

[1] Department of Physics, Baylor University, One Bear Place 97316, Waco, Texas, United States of America
[2] Center for Astrophysics, Space Physics and Engineering Research, 100 Research Parkway, Waco, Texas, United States of America

**E-mail:** Zhiyue_Ding@baylor.edu, Ke_Qiao@baylor.edu and Truell_Hyde@baylor.edu

**Keywords:** complex plasma, mode coupling, nonlinear dynamics

## Abstract

In this paper, we report the first experimental observation of internal resonance in a dusty plasma, which shows the intrinsic nonlinearities of dust interactions in plasmas. When driving a system of vertically aligned dust particle pairs in the vertical direction, the horizontal motion is found to be excited during onset of internal resonance when the higher-frequency horizontal sloshing mode is nonlinearly coupled to the vertical breathing mode through the 1:2 commensurable relation. A theoretical model of the nonlinear interaction of dust particles in plasma is also provided and the results of the theoretical model are shown to match experimental observations.

## 1. Introduction

A dusty plasma is defined as a system where micron-sized particles are immersed in weakly ionized gas. A dusty plasma can act as an analog system for both liquids and solids with the advantage of being able to monitor the motion of each individual dust particle at a fully resolved kinetic level [1, 2]. Dust particles levitating in the plasma sheath region [3, 4] are recognized to exhibit a screened Coulomb interaction [5, 6] and are found to form self-organized structures such as chain structures [7, 8], monolayer crystals [9, 10] and 3D Coulomb balls [5]. The dynamics of the resulting vibrational modes have been studied for these structures, such as the dust-lattice (DL) modes produced in a 1D horizontal chain [11–14], a 2D crystal [15–20] and finite clusters [21]. Mode coupling between the longitudinal and vertical transverse DL mode has also been shown to cause instability and melting [16] for 2D plasma crystals [17–20]. However, these studies have been limited to linear interaction regions, where the resonance between modes occurs only when the modes are at equal frequencies.

In reality, dust particles confined in a plasma sheath are not in a linear environment [22, 23] and the particle–particle restoring interaction [24] is determined by nonlinear functions of displacement. In addition, charge fluctuations can also drive particle motion into the nonlinear regime [25, 26]. Under these conditions, dusty plasma should be considered a nonlinear system where typical nonlinear phenomena, such as internal resonance, should be predictable.

Internal resonance, a type of resonance created by nonlinear mode coupling in systems having multiple degrees of freedom, plays a fundamental role in applications germane to various fields, such as mechanical energy harvesters [27–29], frequency stabilization [30], and nanomechanical systems [31, 32]. A system exhibits internal resonance whenever the natural frequency of two modes satisfies a commensurable relation. In this case, there is a specific ratio (1:2, 1:3, etc) between the frequencies of the coupled modes, or there are specific equality relations among the resonance frequencies of more than two modes, e.g. the resonance frequency of one mode equals the sum of the resonance frequencies of two other modes [33]. Internal resonance can exist for cases with and without external excitations. In the presence of external excitations, the energy in the primary mode that is driven externally increases with increasing excitation amplitude until a saturation point is reached. Beyond this point, the energy begins to be channeled to the secondary mode which is commensurate with the excited mode [34]. In the absence of external excitations, the energy oscillates between the two commensurate

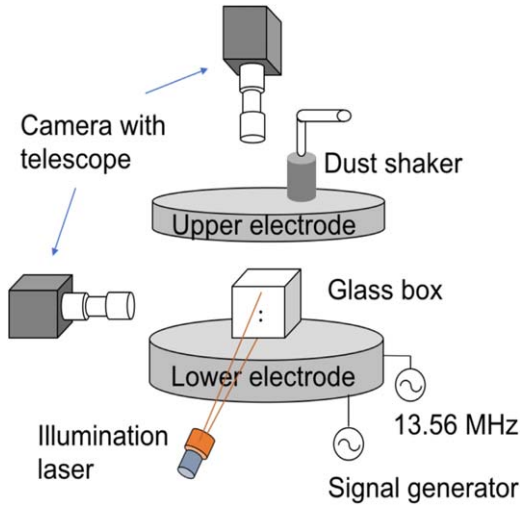


**Figure 1.** Sketch for the experimental setup.

modes [35] (with dissipation in the presence of damping), resulting in a system that is continuously switching between those two modes.

In this paper, we report the first direct observation of internal resonance in a dusty plasma for a dust particle pair vertically aligned along the direction of the ion flow [36–42]. This configuration is the simplest 1D structure involving the ion wake effect [43–45]. Horizontal motion has been found to be excited by a vertical excitation through the 1: 2 internal resonance. The experimental observation is explained by a provided theoretical model, which reveals the intrinsic nonlinearities of the interaction of dust particles in plasmas. As a fundamental phenomena in nonlinear physics, this internal resonance observed in a dusty plasma shows the possibility of dusty plasmas as platforms for studying nonlinear dynamics of liquids and solids at a fully resolved kinetic level.

## 2. Experiment and results

This experiment was conducted in a modified Gaseous Electronics Conference RF reference cell with a lower electrode powered at 13.56 MHz and coupled to a signal generator through an attenuator of 20 dBm in order to allow manipulation of the voltage on the lower electrode (figure 1). A 20 mm $\times$ 18 mm $\times$ 18 mm (height $\times$ length $\times$ width) glass box was placed on the lower electrode to provide the radial confinement necessary to facilitate the formation of the vertical structure examined [46]. All experiments were conducted in argon gas. A vertically aligned pair of melamine formaldehyde particles with particle diameter of 8.89 $\pm$ 0.09 $\mu$m was formed in the plasma inside the glass box by first trapping a cloud of dust particles inside the box and then lowering the plasma power to drop particles until only two particles were left. Illuminated by a laser sheet, the trajectory of these dust particles was recorded by a high speed camera mounted on both the side and the top of the chamber at a frame rate of 250 fps.

As the result of the interaction between the two vertically aligned dust particles, there is a sloshing mode and a breathing mode for the dust pair in the vertical direction which will be referred to as the *S* and the *B* modes in this paper. The same would be expected in the horizontal direction. However, in the experiment, both modes in the horizontal direction become sloshing modes indicating an attractive ion wake interaction [45, 47]. The horizontal sloshing mode with lower resonance frequency will be denoted as the *S*1 mode and the horizontal sloshing mode with higher resonance frequency as the *S*2 mode.

Figure 2 shows the frequency of each of these modes at varying plasma powers and operating pressures.

As shown in figures 2(a) and (b), the frequency of the horizontal *S*2 mode (dark green line) is approximately equal to half that observed for the vertical breathing mode (dashed line) for low pressures (i.e. typically lower than 100 mTorr). For higher pressure (figure 2(c)), the *S*2 mode frequency is significantly less than half of the breathing mode frequency. This indicates that a 1: 2 commensurable relationship between the horizontal *S*2 mode and the vertical *B* mode frequency exists for low pressures.

In order to examine the nonlinear mode coupling and internal resonance, an external sinusoidal voltage of varying amplitude and frequency was applied to the lower electrode providing a vertical excitation to the particle pair. Figures 3(a)–(c) shows the particles' horizontal motion (side view) under an excitation (amplitude of 1.5 V) with frequencies at 13.8, 14.0 and 15.2 Hz (which are close to the *B* mode resonance frequency), at a plasma

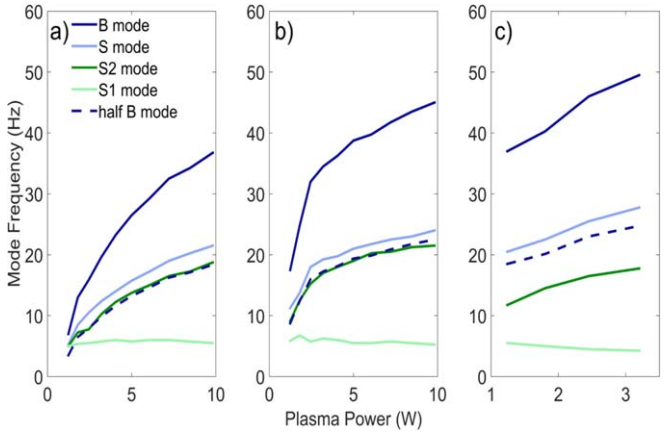


**Figure 2.** Mode frequencies as functions of plasma power at varying pressures (a) 40 mTorr, (b) 80 mTorr, (c) 120 mTorr. Dark blue and light blue lines represent the vertical *B* and *S* modes, while dark green and light green lines show the horizontal *S*2 and *S*1 modes, respectively. The dashed blue line indicates $\frac{1}{2}$ of the frequency of the vertical *B* mode.

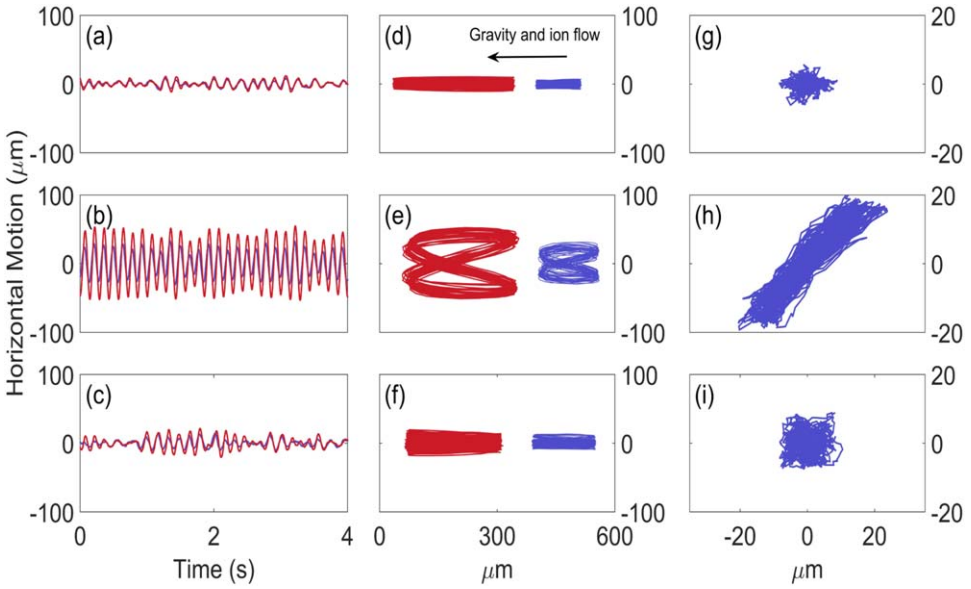


**Figure 3.** Particles' horizontal motion (side view) under a 1.5 V external sinusoidal excitation at (a) 13.8 Hz, (b) 14.0 Hz and (c) 15.2 Hz with the blue line for the upstream particle and red line for the downstream particle. (d)–(f) Corresponding trajectories of both particles recorded from the side view camera. (g)–(i) Corresponding trajectories of the upstream particle recorded from the top view camera.

power of 2.45 W and a pressure of 40 mTorr. The corresponding side-view and top-view trajectories of the upstream particle are shown in figures 3(d)–(f) and (g)–(i), respectively. As shown, the particles exhibit primarily random thermal fluctuation at 13.8 and 15.2 Hz (figures 3(a) and (c)). However, at a driving frequency of 14.0 Hz, a sloshing type horizontal motion having an amplitude of approximately 20 $\mu$m and 40 $\mu$m was excited for the upstream and downstream particle, respectively (figure 3(b)). This clearly shows that the horizontal motion observed is excited through vertical excitation as a result of the onset of an internal resonance at frequency of 14.0 Hz, which is equal to the frequency of the *B* mode and twice that of the *S*2 mode at this pressure and power as shown in figure 2(a).

To illustrate the energy distribution and determine the coupling modes, the power spectra density (PSD) averaged for the horizontal motion over the two particles is shown in figure 4. As can be seen, at an excitation frequency of 14.0 Hz (dark blue line) a significant energy boost is observed centered around 7.1 Hz, the frequency of the *S*2 mode, with no significant increase in the vicinity of the *S*1 mode frequency (~5.0 Hz). This indicates that energy has been transferred into the *S*2 mode which is coupled to the *B* mode through the 1:2 commensurable relationship. It is noticed that this mode coupling between the *S*2 and the *B* mode is not in the linear regime. This is a typical nonlinear mode coupling since the resonance frequencies of the modes are not identical.

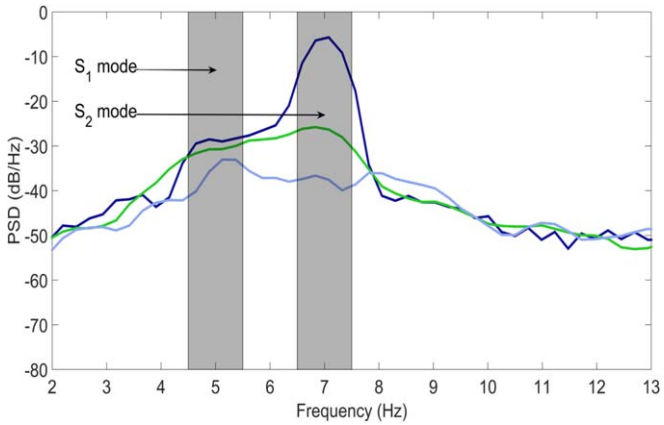


**Figure 4.** The power spectra density (PSD) averaged for the horizontal motion over two dust particles. The dark blue line shows the PSD for a saturated excitation (1.5 V) at a frequency of 14 Hz. The light blue line shows the unsaturated excitation (0.8 V) at the same frequency. The PSD of a saturated excitation (1.5 V) at an off-resonance excitation frequency of 13.8 Hz is shown by the green line.

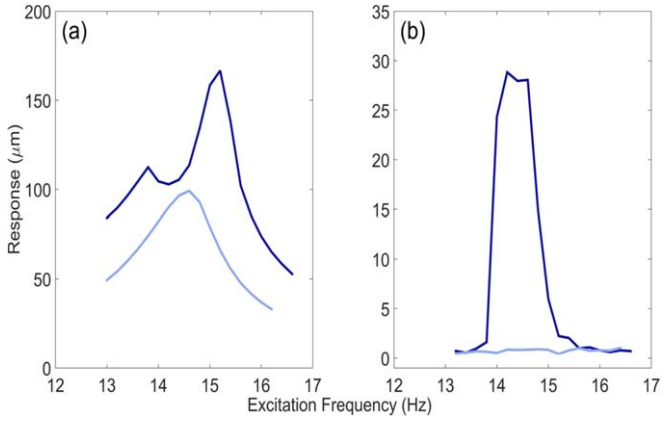


**Figure 5.** Experimentally measured frequency response curves for (a) primary *B* mode and (b) sub-harmonic *S*2 mode. The dark line indicates saturated excitation at 1.5 V, while the light line shows the unsaturated response at 0.8 V.

Such an energy transfer can only be triggered under an external excitation with a large enough amplitude (i.e. saturated excitation). The light blue line in figure 4 shows the averaged PSD for the same experimental conditions but at a driving voltage of 0.8 V. With this unsaturated excitation, no energy boost is observed in the *S*2 mode.

The excitation saturation can be illustrated by experimentally measuring the amplitude-frequency response following the method described in [24]. In this method, particle motions are transferred into the coordinate of each mode employing linear combinations of the original particle trajectories. A Fourier transformation is then implemented on the time series of motion in the new coordinates corresponding to each mode. Primary responses for the *B* mode are measured from the amplitude of the FFT spectrum (of the motion in *B* mode coordinate) at the excitation frequency, while sub-harmonic responses for the *S*2 mode are determined using the amplitude of the FFT spectrum (of the motion in the *S*2 mode coordinate) at half the excitation frequency.

The experimentally measured amplitude-frequency responses of the primary *B* mode and the sub-harmonic *S*2 mode under a plasma power of 2.45 W and a pressure of 40 mTorr are shown in figure 5. As can be seen, at an unsaturated excitation amplitude of 0.8 V (light lines), the primary breathing response curve is smooth and with a single peak unperturbed by internal resonances. Correspondingly, the sub-harmonic *S*2 mode does not show any excitation. At a saturated excitation (1.5 V, dark lines), internal resonance is triggered. Due to this internal resonance, the primary breathing response (dark line in figure 5(a)) decreases while the sub-harmonic *S*2 response (light line in figure 5(b)) increases over the frequency range from approximately 13.8–15.2 Hz, indicating an energy transfer from the *B* to the *S*2 mode. However, there is no sign of such an energy transfer channel existing between the horizontal *S*2 mode and the vertical *B* mode observed for pressures higher than 120 mTorr, where the 1:2 commensurable relation is no longer satisfied.

## 3. Theoretical model

In order to explain the nonlinear mode coupling and internal resonance theoretically, the particle–particle interactions must be investigated to the nonlinear regime and the vertically aligned particles pair are modeled as two coupled oscillators [36, 37, 48, 49] each of which has two degrees of freedom. Horizontal displacements from equilibrium for the upstream and downstream particles are denoted as $x_1$ and $x_2$, and the vertical displacements are $y_1$ and $y_2$. Assuming an equilibrium position with vertical separation of $r_0$ and horizontal separation zero, the particle–particle distance is $r = \sqrt{(x_1 - x_2)^2 + (r_0 + y_1 - y_2)^2}$. A multivariant Taylor series expansion to the second order of the particle–particle interaction force in units of acceleration (normalized by the particle mass) in the general form of a radial function $F(r)$ at equilibrium yields a horizontal component:

$$F_{\text{horizontal}} = \frac{F(r_0)}{r_0}(x_1 - x_2) + \left[\frac{F'(r_0)}{r_0} - \frac{F(r_0)}{r_0^2}\right](x_1 - x_2)(y_1 - y_2), \tag{1}$$

and a vertical component:

$$F_{\text{vertical}} = F(r_0) + F'(r_0)(y_1 - y_2) + \frac{1}{2}\left[\frac{F'(r_0)}{r_0} - \frac{F(r_0)}{r_0^2}\right](x_1 - x_2)^2 + \frac{1}{2}F''(r_0)(y_1 - y_2)^2, \tag{2}$$

where $F(r_0)$, $F'(r_0)$ and $F''(r_0)$ are the zeroth, first and second derivatives of the interaction force with respect to particle–particle spacing $r$ at a vertical equilibrium separation $r_0$, respectively. Due to the non-reciprocal nature [48, 50] of the grain–grain interaction under the influence of the ion wake, the interaction force from downstream particle to upstream particle (denoted by $F_{du}(r)$) is in general not identical to the interaction force from upstream particle to downstream particle (denoted by $F_{ud}(r)$) [36, 37, 51], i.e. $F_{du}(r) \neq F_{ud}(r)$.

The equations of motion for the particle pair aligned along the ion flow with vertical sinusoidal driving force are derived according to the above interaction forces (equation (1) and (2)) with non-reciprocal natural being considered, and have the components in the vertical direction as:

$$\ddot{y}_1 + \mu\dot{y}_1 + \omega_{y1}^2 y_1 + k_{y1}(y_1 - y_2) + L_1(x_1 - x_2)^2 + G_1(y_1 - y_2)^2 = F_1\exp(\mathrm{i}\Omega t) + \text{c.c.}, \tag{3a}$$

$$\ddot{y}_2 + \mu\dot{y}_2 + \omega_{y2}^2 y_2 + k_{y2}(y_2 - y_1) + L_2(x_2 - x_1)^2 + G_2(y_2 - y_1)^2 = F_2\exp(\mathrm{i}\Omega t) + \text{c.c.}, \tag{3b}$$

where $\mu$ is the neutral drag coefficient and $\omega_{y1}$ and $\omega_{y2}$ are the frequencies of the vertical background confinement due to the balance between gravity and the sheath electric field. $F_1, F_2$ are the driving amplitude (in units of acceleration), $\Omega$ is the driving frequency and 'c.c.' stands for the complex conjugate. Meanwhile, the equations of motion in the horizontal direction are

$$\ddot{x}_1 + \mu\dot{x}_1 + \omega_{x1}^2 x_1 + k_{x1}(x_1 - x_2) + M_1(x_1 - x_2)(y_1 - y_2) = 0, \tag{4a}$$

$$\ddot{x}_2 + \mu\dot{x}_2 + \omega_{x2}^2 x_2 + k_{x2}(x_2 - x_1) + M_2(x_1 - x_2)(y_1 - y_2) = 0, \tag{4b}$$

where $\omega_{x1}$ and $\omega_{x2}$ are the frequencies of the horizontal restoring confinement. The driving terms do not appear in the horizontal equations of motion because sinusoidal driving is only applied in the vertical direction.

The connection of the parameters $k_{x1}$, $k_{x2}$, $k_{y1}$, $k_{y2}$, $M_1$, $M_2$, $L_1$, $L_2$ to the interaction forces given by equation (1) and (2) are shown in the table A1 of the appendix. Since $k_{x1}, k_{x2}, k_{y1}, k_{y2}$ and $r_0$ can all be easily measured experimentally (e.g. from the Scanning Mode Spectra [52]), $M_1$,$M_2$, $L_1$ and $L_2$ can in turn also be determined experimentally as $M_1 = 2L_1 = \frac{k_{y1} - k_{x1}}{r_0}$ and $M_2 = 2L_2 = \frac{k_{x2} - k_{y2}}{r_0}$. However, since $G_1$ and $G_2$ depend on the second derivative of the interaction force, they cannot be directly measured experimentally.

The equations of motion equations (3) and (4) are solved in mode coordinates ($q$) by employing the decoupling process [24]:

$$\begin{bmatrix} q_{S2} \\ q_{S1} \\ q_B \\ q_S \end{bmatrix} = \begin{bmatrix} 1 & -\alpha_{S1} & 0 & 0 \\ 1 & -\alpha_{S2} & 0 & 0 \\ 0 & 0 & 1 & -\beta_S \\ 0 & 0 & 1 & -\beta_B \end{bmatrix} \times \begin{bmatrix} x_1 \\ x_2 \\ y_1 \\ y_2 \end{bmatrix}, \tag{5}$$

where $\alpha_{S2}$, $\alpha_{S1}$, $\beta_B$ and $\beta_S$ are the ratios of the oscillation amplitudes of the particles for the corresponding modes. In mode coordinates, the couplings appear only in the nonlinear regime and the corresponding equations of motion are

$$\ddot{q}_{S2} + \mu\dot{q}_{S2} + \omega_{S2}^2 q_{S2} + M_{S2}(C_1 q_{S2} + C_2 q_{S1})(C_3 q_B + C_4 q_S) = 0, \tag{6a}$$

$$\ddot{q}_{S1} + \mu\dot{q}_{S1} + \omega_{S1}^2 q_{S1} + M_{S1}(C_1 q_{S2} + C_2 q_{S1})(C_3 q_B + C_4 q_S) = 0, \tag{6b}$$

$$\ddot{q}_B + \mu\dot{q}_B + \omega_B^2 q_B + L_B(C_1 q_{S2} + C_2 q_{S1})^2 + G_B(C_3 q_B + C_4 q_S)^2 = F_B\exp(\mathrm{i}\Omega t) + \text{c.c.}, \tag{6c}$$

**Table 1.** Model parameters determined for vertically aligned dust pair inside the glass box at a plasma power of 2.45 W and a pressure of 40 mTorr.

| | | | |
|---|---|---|---|
| $\omega_{x1}$ | 5.1(Hz) | $L_1$ | $3.5(\mu m^{-1}\ s^{-2})$ |
| $\omega_{x2}$ | 3.8 | $L_2$ | −2.0 |
| $\omega_{y1}$ | 10.1 | $M_1$ | 7.1 |
| $\omega_{y2}$ | 9.3 | $M_2$ | −4.0 |
| $k_{x1}$ | $-645.0(s^{-2})$ | $\alpha_{S1}$ | 0.74 |
| $k_{x2}$ | 2657.9 | $\alpha_{S2}$ | 0.33 |
| $k_{y1}$ | 1053.3 | $\beta_S$ | 0.88 |
| $k_{y2}$ | 3627.8 | $\beta_B$ | −0.33 |
| $\mu$ | $9.0(s^{-1})$ | $F_1$ | $2.3 \times 10^5(\mu\ ms^{-2})$ |
| $r_0$ | 240.0($\mu$m) | $F_2$ | $2.3 \times 10^5$ |

$$\ddot{q}_S + \mu\dot{q}_S + \omega_S^2 q_S + L_S(C_1 q_{S2} + C_2 q_{S1})^2 + G_S(C_3 q_B + C_4 q_S)^2 = F_S \exp(i\Omega t) + \text{c.c}.. \tag{6d}$$

In the above, the subscripts $S2$, $S1$, and $B$, $S$ correspond to the experimentally observed modes with resonance frequencies denoted by $\omega_{S2}$, $\omega_{S1}$, $\omega_B$ and $\omega_S$. The transformation of the remainder of the parameters can be found in the table A2 of the appendix. We solve equations (6) in the framework of multiple-scale perturbation [35] by introducing a fast scale time $\epsilon t$ where $\epsilon$ is a dimensionless parameter indicating the order of approximation.

Assuming an external driving frequency close to the resonance frequency of the vertical $B$ mode (i.e. $\Omega = \omega_B + \epsilon\delta_1$) and a 1:2 commensurable relation between the $S2$ and $B$ mode (i.e. $2\omega_{S2} = \omega_B + \epsilon\delta_2$), the steady state responses of the $B$ and $S2$ mode (i.e. the response amplitudes $|A_B|$ and $|A_{S2}|$) are determined by eliminating secular terms in the equations of motion to the approximation of order of $O(\epsilon^2)$ and are found to be governed by equations:

$$i\left(2\omega_B\frac{\partial A_B}{\partial \epsilon t} + \mu\omega_B A_B\right) + (L_B C_1^2)A_{S2}^2 \exp(i\epsilon\delta_2 t) - F_B \exp(i\epsilon\delta_1 t) = 0, \tag{7a}$$

$$i(2\omega_{S2}\frac{\partial A_{S2}}{\partial \epsilon t} + \mu\omega_{S2}A_{S2}) + (M_{S2}C_1C_3)A_{S2}^* A_B \exp(-i\epsilon\delta_2 t) + \left(\frac{F_S M_{S2} C_1 C_4}{-\Omega^2 + \omega_S^2}\right)A_{S2}^* \exp(i\epsilon\delta_1 t - i\epsilon\delta_2 t) = 0, \tag{7b}$$

where $A_{S2}^*$ is the complex conjugate of $A_{S2}$. Note that the second term $(L_B C_1^2)A_{S2}^2 \exp(i\epsilon\delta_2 t)$ in equation (7a) and the second term $(M_{S2}C_1C_3)A_{S2}^* A_B \exp(-i\epsilon\delta_2 t)$ in equation (7b) are caused by the nonlinearity, while the third term $\left(\frac{F_S M_{S2} C_1 C_4}{-\Omega^2 + \omega_S^2}\right)A_{S2}^* \exp(i\epsilon\delta_1 t - i\epsilon\delta_2 t)$ in equation (7b) is due the non-reciprocal nature of the interaction as it goes to zero when the interactions become reciprocal (see equations (9) in the discussion section). On the other hand, without presuming the commensurable relationship $2\omega_{S2} = \omega_B + \epsilon\delta_2$, the governing equations are

$$i\left(2\omega_B\frac{\partial A_B}{\partial \epsilon t} + \mu\omega_B A_B\right) - F_B \exp(i\epsilon\delta_1 t) = 0, \tag{8a}$$

$$2\frac{\partial A_{S2}}{\partial \epsilon t} + \mu A_{S2} = 0. \tag{8b}$$

Equations (8) can be solved analytically while equations (7) must be solved numerically (due to the coupling between $A_B$ and $A_{S2}$). This is most easily accomplished by substituting the test solutions $A_B = |A_B|e^{i\theta_B}$ and $A_{S2} = |A_{S2}|e^{i\theta_{S2}}$ and separately equating the real and imaginary parts of the resulting equations.

The parameters needed to determine solutions for equations (7) and (8) are given in table 1, which are consistent with the result from Carstensen *et al* [36] in that the downstream particle yields lower confinement frequencies (e.g. $\omega_{y2} < \omega_{y1}$) but larger linear coupling constants (e.g. $k_{y2} > k_{y1}$). The excitation amplitudes $F_1$ and $F_2$ are estimated to be $2.3 \times 10^5 \mu m\ s^{-2}$ for an excitation amplitude of 1.5 $V$ with discrepancies between $F_1$ and $F_2$ being ignored. The neutral drag coefficient set to be $9.0\ s^{-1}$ as a reasonable value at the plasma pressure of 40 mTorr [53].

Using the model parameters determined from the experiment, steady-state responses are solved, and are shown in figure 6. Solutions of equations (7), in which the $S2$ and $B$ modes are assumed to be commensurable, are shown by the solid lines for both saturated (dark lines) and unsaturated (light lines, where $F_1 = F_2 = 1.2 \times 10^5\ \mu m\ s^{-2}$ for an experiment amplitude of 0.8 V) responses. As shown, the energy transfer from the $B$ to the $S2$ mode is observed over the same frequency range as in the experiment (figure 5). The excitation of the $S2$ mode and the depression of the $B$ mode are successfully predicted. Without the assumption of the commensurate relationship, the solution to equations (8), shown in red, shows no energy transfer from the $B$ to the $S2$ mode.

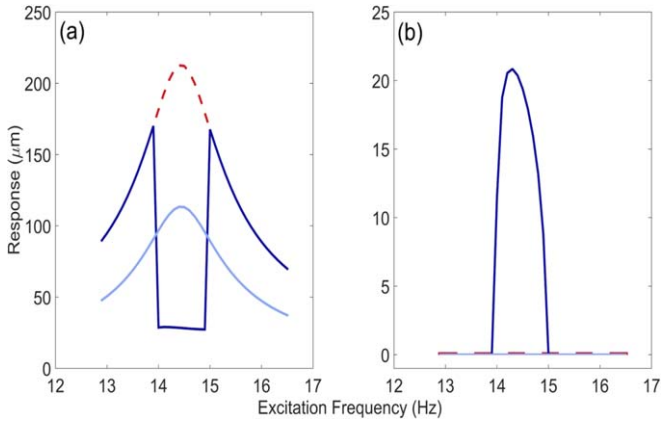


**Figure 6.** The theoretical response curves for (a) primary *B* mode, (b) sub-harmonic *S*2 mode. The dark blue lines and red dashed lines are the responses under a saturated excitation with and without the assumption that the *S*2 and the *B* mode are 1:2 commensurable. The light blue lines are the response curves under an unsaturated excitation.

## 4. Discussion

Comparing equations (7) and (8), the energy loss for the *B* mode can be attributed to the term $(L_B C_1^2)A_{S2}^2 \exp(\mathrm{i}\epsilon\delta_2 t)$ in equation (7*a*), whose magnitude is determined by the amplitude of the *S*2 mode ($A_{S2}^2$) and the coupling strength $L_B C_1^2$, while the excitation of the *S*2 mode can be attributed to the last two terms in equation (7*b*). The first of these terms is a direct consequence of internal resonance, i.e. the coupling of the *S*2 mode to the *B* mode, whose magnitude is determined by the amplitude of the *B* mode response $A_B$, as well as the coupling strength $M_{S2} C_1 C_3$. The second term is due to the coupling of the *S*2 mode to the *S* mode. However, since the *S* mode is not in resonance with the external excitation, its primary response is of the form $\frac{F_S}{-\Omega^2+\omega_S^2}$. Thus, this term can be understood as the coupling between the *S*2 mode and the external excitation. Experimentally, at external excitation frequencies close to the resonance frequency of the *B* mode (i.e. between 13 and 16.5 Hz), the magnitude of the first term proportional to $M_{S2} C_1 C_3 A_B$ ($\approx 10^3\ \mathrm{s}^{-2}$) is one order greater than the magnitude of the second term proportional to $\frac{F_S M_{S2} C_1 C_4}{-\Omega^2+\omega_S^2}$ ($\approx 10^2\ \mathrm{s}^{-2}$), i.e. the ratio $(M_{S2} C_1 C_3 A_B) \Big/ \left(\frac{F_S M_{S2} C_1 C_4}{-\Omega^2+\omega_S^2}\right)$ is in the range 8−24. Therefore, the majority of the energy gained by the *S*2 mode comes from the coupling established between the *S*2 mode and the *B* mode, while the loss of the energy of the *B* mode is solely caused by nonlinear coupling between the *B* mode and the *S*2 mode. As such, the discrepancy between the magnitude of the experimental and theoretical response curves (especially for the *B* mode) could be due to other coupling resonances not considered in this model. The best likely of these is a coupling between the vertical *S* and *B* mode given the resonance frequencies of the *S* mode are approximate half that of the *B* mode (figure 2). Also, the assumption of the radial interaction function $F(r)$ has a limited capability of describing the possible non-radial effects of the interaction (e.g. the effect of the ion drag), especially for the downstream interaction where more sophisticated wake potential models based on ion knentic theory have been presented [54–56]. In this case, the assumption of the radial interaction function also might lead to this discrepancy.

It is helpful to discuss the reciprocal interaction case as a baseline for understanding nonlinear mode couplings. Considering the situation when the grain–grain interaction is reciprocal (i.e. $F_{du} = F_{ud}$) and ignoring the difference between the background confinements for both particles (i.e. $\omega_{x1} = \omega_{x2}, \omega_{y1} = \omega_{y2}$) yields perfect sloshing ($\alpha_{S1} = \beta_S = 1$) and perfect breathing ($\alpha_{S2} = \beta_B = -1$) modes in both the horizontal and vertical directions (i.e. the *S*2 mode in the horizontal direction becomes a breathing type mode *Bx*). As such, the model presented reduces to (in decoupled mode coordinates):

$$\ddot{q}_{Bx} + \mu\dot{q}_{Bx} + \omega_{Bx}^2 q_{Bx} + 2M_1 q_{Bx} q_{By} = 0, \tag{9a}$$

$$\ddot{q}_{Sx} + \mu\dot{q}_{Sx} + \omega_{Sx}^2 q_{Sx} = 0, \tag{9b}$$

$$\ddot{q}_{By} + \mu\dot{q}_{By} + \omega_{By}^2 q_{By} + 2L_1 q_{Bx}^2 + 2G_1 q_{By}^2 = F_{By}\exp(\mathrm{i}\Omega t) + \mathrm{cc}, \tag{9c}$$

$$\ddot{q}_{Sy} + \mu\dot{q}_{Sy} + \omega_{Sy}^2 q_{Sy} = F_{Sy}\exp(\mathrm{i}\Omega t) + \mathrm{cc}, \tag{9d}$$

where *Bx* and *Sx* represent the horizontal breathing and sloshing modes, and *By* and *Sy* represent the vertical breathing and sloshing modes. Equation (9*b*) and (9*d*) show that the sloshing modes (*Sx* and *Sy*) in both directions are isolated, i.e. there is no coupling (neither linearly nor nonlinearly) between them to other modes in the system. Therefore, in the current experiment, any nonlinear coupling involving the horizontal *S*1 or

vertical *S* mode (low frequency sloshing type modes that characterize the environment background confinements), for example, the coupling between the *S*2 and the *S* mode given by the last term in equation (7*b*), would be the direct result of the nonreciprocal interaction due to the ion wake effect.

In the actual experimental environment, the particles' dynamics are not only affected by the quadratic nonlinearities that were considered in this research, but also by cubic nonlinearities. As direct evidence of the existence of cubic nonlinearities in the system, the 'spring hardening' phenomenon (i.e. the response curve being 'bent' towards the higher frequencies) is observed for the primary breathing response curve (see figure 5(a)). However, cubic nonlinearities do not cause any internal resonance since there is no 1:3 commensurable relationship between any of the modes in this system.

An internal resonance, although never investigated in dusty plasma before, should be a ubiquitous phenomenon. For example, it may play a role in the bistable switching phenomenon reported recently for 2D clusters [57]. In this case, the continuous switching between gas-like random motion and vertical oscillations of the condensed crystal lattice may be triggered due to an internal resonance between the in-plane and out-of-plane modes whose frequencies are not necessarily identical. This is bolstered by the perfect periodic kinetic energy fluctuations in the horizontal direction (figure 2(k) in [57]) that resembles the continuous periodic energy exchange occuring during internal resonance in an unexcited system.

## 5. Summary

In this paper, the first experimental observation of the 1: 2 internal resonance is reported in dusty plasma, for a vertical dust pair, between the horizontal *S*2 mode and the vertical *B* mode. Under low plasma pressures, these two modes become 1:2 commensurable, in which case the horizontal *S*2 mode is found to be excited by vertical driving with frequencies at the resonance frequency of the *B* mode at sufficiently large driving amplitude. Both the PSD and the amplitude-frequency response curves obtained from the particle motion show a clear energy transfer from the *B* mode to the *S*2 mode. A theoretical model has also been established for vertical pair structures with non-reciprocal interactions where the quadratic terms and the coupling between vertical and horizontal motions were also considered. The 1:2 internal resonance was theoretically illustrated by solving the model employing a multiple scale perturbation method. The theoretical response curves were calculated for the onset of internal resonance and show excellent agreement with experimental results. The nonlinear couplings of the system of dust particles to the plasma environment (characterized by the low frequency sloshing type mode couplings) are found to be caused by the influence of the ion wake.

This observation of internal resonance as a result of nonlinear mode coupling reveals the intrinsic nonlinearities of the interaction of dust particles in plasmas, which also shows the capability of dusty plasmas as platforms for study nonlinear dynamics of liquids and solids at a fully resolved kinetic level in the future.

## Acknowledgments

Support from NASA grant number 1571701 and NSF grant number 1740203 is gratefully acknowledged.

## Appendix

Reference tables for model parameters in equations (3), (4) and (6).

**Table A1.** Reference table for parameters in equations (3) and (4). The subscriptions *du* and *ud*, respectively, refer to the interaction from the downstream particle to the upstream particle and the interaction from the upstream particle to the downstream particle. Due to the non-reciprocal nature of the interaction, the upstream interaction needs to be treated separately from the downstream interaction.

| | |
|---|---|
| $k_{x1} = -\frac{F_{du}(r_0)}{r_0}$ | $M_1 = 2L_1 = \frac{F_{du}(r_0)}{r_0^2} - \frac{F'_{du}(r_0)}{r_0}$ |
| $k_{x2} = -\frac{F_{ud}(r_0)}{r_0}$ | $M_2 = 2L_2 = -\left(\frac{F_{ud}(r_0)}{r_0^2} - \frac{F'_{ud}(r_0)}{r_0}\right)$ |
| $k_{y1} = -F'_{du}(r_0)$ | $G_1 = -\frac{1}{2}F_{du}''(r_0)$ |
| $k_{y2} = -F'_{ud}(r_0)$ | $G_2 = \frac{1}{2}F_{ud}''(r_0)$ |

**Table A2.** Reference table for the transformation of parameters from the original coordinates (equations (3) and (4)) to the mode coordinates (equations (6)).

| | | |
|---|---|---|
| $M_{S2} = M_1 - \alpha_{S1} M_2$ | $G_B = G_1 - \beta_S G_2$ | $C_1 = \frac{\alpha_{S2} - 1}{\alpha_{S2} - \alpha_{S1}}$ |
| $M_{S1} = M_1 - \alpha_{S2} M_2$ | $G_S = G_1 - \beta_B G_2$ | $C_2 = \frac{1 - \alpha_{S1}}{\alpha_{S2} - \alpha_{S1}}$ |
| $L_B = L_1 - \beta_S L_2$ | $F_B = F_1 - \beta_S F_2$ | $C_3 = \frac{\beta_B - 1}{\beta_B - \beta_S}$ |
| $L_S = L_1 - \beta_B L_2$ | $F_S = F_1 - \beta_B F_2$ | $C_4 = \frac{1 - \beta_S}{\beta_B - \beta_S}$ |

## ORCID iDs

Zhiyue Ding https://orcid.org/0000-0003-1554-5911

## References


[1] Fortov V, Ivlev A, Khrapak S, Khrapak A and Morfill G 2005 *Phys. Rep.* **421** 1–103
[2] Morfill G E and Ivlev A V 2009 *Rev. Mod. Phys.* **81** 1353–404
[3] Trottenberg T, Melzer A and Piel A 1995 *Plasma Sources Sci. Technol.* **4** 450
[4] Panagopoulos T and Economou D J 1999 *J. Appl. Phys.* **85** 3435–43
[5] Arp O, Block D, Piel A and Melzer A 2004 *Phys. Rev. Lett.* **93** 165004
[6] Antonova T, Annaratone B M, Goldbeck D D, Yaroshenko V, Thomas H M and Morfill G E 2006 *Phys. Rev. Lett.* **96** 115001
[7] Liu B and Goree J 2005 *Phys. Rev.* E **71** 046410
[8] Kong J, Hyde T W, Matthews L, Qiao K, Zhang Z and Douglass A 2011 *Phys. Rev.* E **84** 016411
[9] Goree J, Samsonov D, Ma Z, Bhattacharjee A, Thomas H, Konopka U and Morfill G 2000 *Monolayer Plasma Crystals: Experiments and Simulations* (*Frontiers in Dusty Plasmas* ) (Amsterdam: Elsevier) pp 91–7
[10] Vaulina O S, (Adamovich) X G K and Vladimirov S V 2009 *Phys. Scr.* **79** 035501
[11] Ivlev A V and Morfill G 2000 *Phys. Rev.* E **63** 016409
[12] Yaroshenko V V, Ivlev A V and Morfill G E 2005 *Phys. Rev.* E **71** 046405
[13] Liu B, Goree J and Feng Y 2010 *Phys. Rev. Lett.* **105** 085004
[14] Qiao K, Kong J, Matthews L S and Hyde T W 2015 *Phys. Rev.* E **91** 053101
[15] Zhdanov S K, Ivlev A V and Morfill G E 2009 *Phys. Plasmas* **16** 083706
[16] Couëdel L, Zhdanov S K, Ivlev A V, Nosenko V, Thomas H M and Morfill G E 2011 *Phys. Plasmas* **18** 083707
[17] Melzer A, Schweigert V A, Schweigert I V, Homann A, Peters S and Piel A 1996 *Phys. Rev.* E **54** R46–9
[18] Schweigert V A, Schweigert I V, Melzer A, Homann A and Piel A 1998 *Phys. Rev. Lett.* **80** 5345–8
[19] Ivlev A V, Konopka U, Morfill G and Joyce G 2003 *Phys. Rev.* E **68** 026405
[20] Couëdel L, Nosenko V, Ivlev A V, Zhdanov S K, Thomas H M and Morfill G E 2010 *Phys. Rev. Lett.* **104** 195001
[21] Qiao K, Kong J, Carmona-Reyes J, Matthews L S and Hyde T W 2014 *Phys. Rev.* E **90** 033109
[22] Ivlev A V, Sütterlin R, Steinberg V, Zuzic M and Morfill G 2000 *Phys. Rev. Lett.* **85** 4060–3
[23] Sorasio G, Resendes D and Shukla P 2002 *Phys. Lett.* A **293** 73
[24] Ding Z, Qiao K, Kong J, Matthews L S and Hyde T W 2019 *Plasma Phys. Control. Fusion* **61** 055004
[25] Wang Y N, Hou L J and Wang X 2002 *Phys. Rev. Lett.* **89** 155001
[26] Zafiu C, Melzer A and Piel A 2001 *Phys. Rev.* E **63** 066403
[27] Cottone F, Vocca H and Gammaitoni L 2009 *Phys. Rev. Lett.* **102** 080601
[28] Xu J and Tang J 2015 *Appl. Phys. Lett.* **107** 213902
[29] Xiong L, Tang L and Mace B R 2016 *Appl. Phys. Lett.* **108** 203901
[30] Antonio D, Zanette D H and López D 2012 *Nat. Commun.* **3** 806 EP
[31] Samanta C, Yasasvi Gangavarapu P R and Naik A K 2015 *Appl. Phys. Lett.* **107** 173110
[32] Chen C, Zanette D H, Czaplewski D A, Shaw S and López D 2017 *Nat. Commun.* **8** 15523 EP
[33] Sethna P R and Bajaj A K 1978 *J. Appl. Mech.* **45** 895–902
[34] Sayed M and Kamel M 2012 *Appl. Math. Modelling* **36** 310–32
[35] Nayfeh A H and Mook D T 1979 *Nonlinear Oscillations* (New York: Wiley) pp 365–443
[36] Carstensen J, Greiner F, Block D, Schablinski J, Miloch W J and Piel A 2012 *Phys. Plasmas* **19** 033702
[37] Jung H, Greiner F, Asnaz O H, Carstensen J and Piel A 2015 *Phys. Plasmas* **22** 053702
[38] Lampe M, Joyce G and Ganguli G 2005 *IEEE Trans. Plasma Sci.* **33** 57–69
[39] Piel A 2011 *Phys. Plasmas* **18** 073704
[40] Block D, Carstensen J, Ludwig P, Miloch W, Greiner F, Piel A, Bonitz M and Melzer A 2012 *Contrib. Plasma Phys.* **52** 804–12
[41] Ludwig P, Miloch W J, Kählert H and Bonitz M 2012 *New J. Phys.* **14** 053016
[42] Hutchinson I H 2012 *Phys. Rev.* E **85** 066409 Pt 2
[43] Ishihara O and Vladimirov S V 1997 *Phys. Plasmas* **4** 69–74
[44] Lemons D S, Murillo M S, Daughton W and Winske D 2000 *Phys. Plasmas* **7** 2306–13
[45] Nosenko V, Ivlev A V, Kompaneets R and Morfill G 2014 *Phys. Plasmas* **21** 113701
[46] Kong J, Qiao K, Matthews L S and Hyde T W 2014 *Phys. Rev.* E **90** 013107
[47] Melzer A, Schweigert V and Piel A 1999 *Phys. Rev. Lett.* **83** 3194
[48] Hebner G A and Riley M E 2004 *Phys. Rev.* E **69** 026405
[49] Melzer A, Schweigert V A and Piel A 2000 *Phys. Scr.* **61** 494–501
[50] Melzer A 2001 *Phys. Scr.* **T89** 33

[51] Ivlev A V, Bartnick J, Heinen M, Du C R, Nosenko V and Löwen H 2015 *Phys. Rev.* X **5** 011035
[52] Qiao K, Ding Z, Kong J, Chen M, Matthews L S and Hyde T W 1705 (arXiv:1705.01982)
[53] Douglass A, Land V, Qiao K, Matthews L and Hyde T 2016 *J. Plasma Phys.* **82** 1–10
[54] Kompaneets R, Konopka U, Ivlev A V, Tsytovich V and Morfill G 2007 *Phys. Plasmas* **14** 052108
[55] Kompaneets R, Morfill G E and Ivlev A V 2016 *Phys. Rev.* E **93** 063201
[56] Kompaneets R, Morfill G E and Ivlev A V 2016 *Phys. Rev. Lett.* **116** 125001
[57] Gogia G and Burton J C 2017 *Phys. Rev. Lett.* **119** 178004